Research Square

Preprints are preliminary reports that have not undergone peer review.
They should not be considered conclusive, used to inform clinical practice,
or referenced by the media as validated information.

An In Vivo Model of Ischemic Spinal Cord Injury in Awake Rats Identifies Early Mixed Macrophage Polarization and Impaired Inflammatory Resolution

Renato Rozental

renato.rozental@fiocruz.br

Fundação Oswaldo Cruz (Fiocruz) https://orcid.org/0000-0003-0092-6076

Tagore de Morais

Caio Perret

https://orcid.org/0000-0003-1769-2034

Karsten Gronert

Fred Lado

Article

Keywords: awake animal model; maximal electroshock seizures (MES); ischemic spinal cord injury (iSCI); Specialized Pro-Resolving Mediators (SPMs); inflammation; cerebrospinal fluid (CSF); Monocyte chemoattractant protein-1 (MCP-1)

Posted Date: November 20th, 2026

DOI: https://doi.org/10.21203/rs.3.rs-11273532/v1

License: This work is licensed under a Creative Commons Attribution 4.0 International License.
Read Full License

Additional Declarations: There is no duality of interest

MS #1: Animal model, cellular architecture and early gene expression
back-to-back submission

An In Vivo Model of Ischemic Spinal Cord Injury in Awake Rats Identifies Early Mixed Macrophage Polarization and Impaired Inflammatory Resolution

[1]Tagore G. de Morais[¶],[1]Caio Perret[¶], [2]Karsten Gronert, [3]Fred A. Lado, [1,4,5]Renato Rozental[*].

[¶] *contributed equally to this work*

[1]Instituto de Ciências Biomédicas, CCS, Universidade Federal do Rio de Janeiro, 21941-902, Brazil
[2]Herbert Wertheim School of Optometry & Vision Science, University of California, Berkeley, CA, 94720-2020, USA.
[3]Dept Neurology, Zucker School of Medicine at Hofstra-Northwell, Great Neck, NY, 11021, USA
[4]Centro Desenvolvimento Tecnológico (CDTS) & Instituto Oswaldo Cruz (IOC), FIOCRUZ, Rio de Janeiro, 21040-361, Brazil
[5]Dept Neuroscience, Albert Einstein Coll Medicine, Bronx, NY, 10461, USA

[*]Corresponding author:
Renato Rozental, *MD, PhD*
renato.rozental@fiocruz.br

Fundação Oswaldo Cruz - FIOCRUZ
Centro de Desenvolvimento Tecnológico em Saúde (*CDTS*)
Térreo – r. 06
Av. Brasil 4365, Campus Manguinhos
Manguinhos, Rio de Janeiro, 21040-360
Brasil

Keywords: awake animal model; maximal electroshock seizures (MES); ischemic spinal cord injury (iSCI); Specialized Pro-Resolving Mediators (SPMs); inflammation; cerebrospinal fluid (CSF); Monocyte chemoattractant protein-1 (MCP-1).

ILLUSTRATIONS:

- 3 MAIN FIGURES (figure legends appear after the References section)
- 4 SUPPLEMENTARY FIGURES (*Supporting Information*)

ABSTRACT

Study Design: Animal study. Female Sprague-Dawley rats.

Objectives: To establish an awake, anesthesia-free rat model of ischemic spinal cord injury (SCI) and characterize the molecular and cellular mechanisms associated with lesion progression during the first 24 h after paralysis.

Setting: Brazil and USA.

Methods: Ischemic SCI was induced in awake rats by repeated transauricular maximal electroshock seizures (MES). Neurological function, magnetic resonance imaging (MRI), histopathology, cellular responses, and transcriptomic profiles were evaluated during the acute and early subacute phases after injury.

Results: Repeated MES produced reproducible thoracic (T8–T12) watershed infarcts predominantly involving the anterior spinal cord, with bilateral “owl’s-eye” lesions on MRI, paralysis below T9–T10, and progressive tissue vacuolization between days 3 and 5. Integrated cellular, molecular, and transcriptomic analyses revealed early monocyte recruitment, dysregulated inflammatory signaling, mixed macrophage-associated phenotypes, impaired inflammatory resolution, and limited astrocytic response. Transcriptomic profiling identified activation of the DHA–lipoxygenase pathway associated with endogenous inflammatory resolution, whereas genes involved in astrocytic DHA biosynthesis were downregulated by 24 h, suggesting a temporal mismatch between pro-resolving signaling and substrate availability for specialized pro-resolving lipid mediator biosynthesis.

Conclusions: An awake, anesthesia-free model of SCI reproduces key pathological and clinically relevant features of human ischemic SCI and reveals early dysregulation of the inflammatory–lipid resolution axis. These findings identify impaired coordination between inflammatory signaling and endogenous lipid-mediated resolution as a potential mechanism contributing to secondary lesion progression and provide a platform for evaluating time-sensitive neuroprotective interventions.

Sponsorship: FAPERJ; Brazilian Ministry of Health; and NY State SCI Research.

INTRODUCTION

Spinal cord injury (SCI) remains a devastating neurological condition that frequently results in permanent motor, sensory, and autonomic dysfunction. Although the primary mechanical or ischemic insult initiates tissue damage, neurological deterioration is largely driven by a complex cascade of secondary injury mechanisms that evolves over hours to days after injury, including vascular dysfunction, excitotoxicity, oxidative stress, inflammation, and progressive cell death[1]. Considerable advances have been made in characterizing the subacute and chronic phases of SCI; however, the molecular and cellular events occurring during the first 24 h after injury - when lesion expansion is likely most dynamic and potentially amenable to therapeutic intervention - remain incompletely understood. Consequently, efforts to target acute injury-phase mechanisms have yielded limited and often inconsistent clinical benefit.

A major challenge in defining these early pathogenic events has been the reliance on experimental SCI models requiring anesthesia and invasive surgical procedures. Both factors profoundly influence neurovascular coupling, systemic physiology, immune activation, and glial responses, thereby introducing important confounders into studies of acute injury biology[2,3]. These limitations are particularly relevant when investigating neuroinflammatory processes, which are highly sensitive to alterations in neural activity, blood flow, and immune regulation. Experimental systems capable of capturing the immediate response to SCI in the absence of these modifiers are therefore needed to improve understanding of the mechanisms governing early lesion evolution.

Inflammation is increasingly recognized as a central determinant of secondary tissue damage after SCI. Following injury, resident microglia are rapidly activated and accompanied by recruitment of neutrophils, monocyte-derived macrophages, and lymphocyte populations that collectively shape the local inflammatory milieu[4]. While these responses contribute to debris clearance and tissue remodeling, they can also amplify neuronal and glial injury through sustained production of cytokines, chemokines, reactive oxygen species, and bioactive lipid mediators[5]. Among immune cell populations, macrophages and microglia have emerged as major regulators of lesion progression owing to their remarkable phenotypic heterogeneity and capacity to coordinate both inflammatory and reparative programs[6]. Temporal profiling studies have demonstrated persistent leukocyte accumulation within the injured SC for weeks after injury, with resolution-associated pathways becoming increasingly prominent during later stages of lesion evolution[7]. This dynamic inflammatory landscape provided the biological rationale for the use of high-dose corticosteroids in acute SCI as a means of limiting secondary injury through suppression of inflammatory amplification[8,9]. However, despite decades of investigation, the efficacy of corticosteroid therapy remains controversial, highlighting an incomplete understanding of the temporal relationship between inflammatory injury and endogenous repair and underscoring the need to identify more precise therapeutic targets within the early inflammatory response.

Recent advances have challenged the traditional view of post-traumatic inflammation as a purely pathological and self-limiting process. Specialized pro-

resolving mediators (SPMs), a family of bioactive lipid mediators derived from polyunsaturated fatty acids, actively orchestrate the resolution of inflammation and restoration of tissue homeostasis in multiple neurological disorders[10,11]. Rather than suppressing immune responses indiscriminately, SPMs promote coordinated termination of inflammation through regulation of leukocyte trafficking, enhancement of phagocytosis and efferocytosis, and activation of tissues repair programs. Within the injured CNS, astrocytes, macrophages, and microglia constitute key components of these pathways, functioning as major producers, responders, and effectors of SPM signaling[12–15]. Astrocytes contribute to the biosynthesis and mobilization of docosahexaenoic acid (DHA)-derived mediators, whereas macrophages and microglia integrate pro-resolving signals that regulate inflammatory activation, debris clearance, and restoration of tissue homeostasis. Despite increasing recognition of the importance of resolution biology in CNS injury, the temporal dynamics and cellular regulation of these pathways during the earliest stages of SCI remain poorly defined. It is unknown whether acute SCI is characterized by effective activation of endogenous resolution mechanisms or by failure to initiate and sustain pro-resolving responses. Defining how these cellular networks coordinate inflammatory resolution during the first hours after injury is therefore critical for understanding the balance between secondary tissue damage and repair and for identifying therapeutic strategies capable of promoting neurological recovery.

To address these questions, we developed an anesthesia-free rat model of ischemic SCI induced by repeated transauricular maximal electroshock seizures (MES). This model produces reproducible thoracolumbar watershed infarcts with selective gray matter vulnerability and recapitulates key radiological, histopathological, and functional features of human disease. Using integrated transcriptomic, proteomic, lipidomic, histological, and electrophysiological analyses, we define the molecular and cellular landscape of the first 24 h after injury. We identify rapid MCP-1-associated monocyte recruitment, early macrophage predominance, heterogeneous inflammatory activation states, and evidence of defective engagement of endogenous resolution pathways. Notably, these alterations are accompanied by suppression of astrocytic programs involved in lipid metabolism and biosynthesis of pro-resolving mediators, including components of the DHA-lipoxygenase axis, suggesting that impaired inflammatory resolution may represent a previously underappreciated driver of lesion expansion during acute ischemic SCI. Together, these findings establish the early molecular architecture of ischemic SCI in an anesthesia-free context and provide a mechanistic framework for understanding how dysregulated inflammatory resolution contributes to secondary injury progression.

MATERIAL AND METHODS

Repeated maximal electroshock seizure (MES) paradigm. The experimental paradigm was developed from classical transauricular MES models described by Isaac and Advokat and subsequently incorporated into established descriptions of generalized seizures in freely moving rodents[16–18]. We modified this established paradigm by modifying the stimulation parameters and incorporating pregnancy as an experimental condition to convert the previously described

transient motor phenotype into a reproducible and persistent neurological deficit associated with ischemic SCI.

A total of 172 Sprague–Dawley rats were included in the study, comprising 140 pregnant rats subjected to repeated MES stimulation, 20 pregnant control rats receiving subthreshold stimulation, and an age-matched cohort of 12 non-pregnant female rats subjected to MES stimulation. Pregnant Sprague–Dawley rats (2–3 months old, 200–250 g; Taconic Farms, Germantown, NY, USA; *n* = 140) received transauricular electrical stimulation through bilateral ear-clip electrodes connected to a constant-voltage stimulator (Grass Instruments, Model S48, Quincy, MA, USA). An age-matched cohort of non-pregnant female Sprague–Dawley rats (*n* = 12) underwent the identical stimulation protocol to assess the contribution of pregnancy-associated physiological adaptations to the development of seizure-induced ischemic SCI. Control animals consisted of pregnant Sprague–Dawley rats (*n* = 20) that underwent identical handling and electrode placement but received subthreshold stimulation (15 V), which did not induce generalized seizures. Animals were briefly restrained for electrode placement and subsequently stimulated while awake. Each stimulation session consisted of four consecutive maximal electroshock seizures (MES) delivered at 30-s intervals. Animals underwent one stimulation session during the first experimental week, four sessions during the second week, and seven sessions during the third week. See ***SI Materials and Methods*** *for details*.

To estimate the effective current generated under the experimental conditions, transauricular current measurements were measured in seven animals randomly selected from the reported MES cohort that did not develop paralysis (MES-stimulated non-paralyzed animals). Measurements were performed immediately after euthanasia at the end of the fifth experimental day. The ear-clip electrodes were maintained in their original positions, and the stimulation parameters used in the experimental protocol (120 V, 50 Hz, 2 s) were reapplied while current was measured across the transauricular circuit. Recorded currents ranged from 90 to 137 mA, corresponding to transauricular impedances of 875–1330 Ω as calculated according to Ohm's law. These measurements experimentally defined the current delivered across the transauricular pathway under the electrode configuration and stimulation conditions used in the MES paradigm[19]**.** Generalized tonic–clonic seizures were defined by the stereotypical behavioral sequence elicited by MES, consisting of tonic flexion, tonic hindlimb extension (THE; bilateral hindlimb extension to approximately 180° relative to the longitudinal body axis), followed by generalized clonic convulsions and postictal depression. The occurrence of complete THE or tonic flexion was used as the primary criterion for successful seizure induction. Animals were continuously monitored throughout each stimulation session and until recovery of spontaneous locomotor activity before being returned to their home cages. See ***SI Materials and Methods*** *for details*.

X-Ray (Siemens) and Magnetic Resonance Imaging (MRI) (T2-weighted).
X-ray imaging (Siemens) (n = 5) and T2-weighted magnetic resonance imaging (MRI) (n = 2) were performed to substantiate characterizing of SC pathology following MES. MRI was acquired using a high-field 9.4 T Varian system (Agilent Technologies, Santa Clara, CA, USA), following established small-animal MRI

approaches for experimental neuroimaging and rodent SC imaging at the Gruss Magnetic Resonance Research Center (MRRC) at the Albert Einstein College of Medicine. Multislice spin-echo T2-weighted images were acquired of the brain and SC using a repetition time (TR) of 1.5 s and echo time (TE) of 40 ms, with a slice thickness of 1 mm. See ***SI Materials and Methods*** *for details*.

Profile of gene expression 24h after paralysis

Tissue collection and RNA preparation for microarray analysis. At 24 h after the onset of paralysis, nine independent biological samples were collected for transcriptomic analysis, comprising three uninjured controls, three MES-stimulated non-paralyzed animals, and three MES-stimulated paralyzed animals, with the latter two groups time-matched. Animals were deeply anesthetized and euthanized, and thoracic SC segments T8–T12, encompassing the T10 lesion epicenter, were rapidly dissected under RNase-free conditions within 3–5 min of euthanasia. Tissue was immediately transferred to sterile RNase-free cryovials, snap-frozen in liquid nitrogen, and stored at −80 °C until analysis. Samples were transported on dry ice to Genome Explorations (Memphis, TN, USA) without freeze–thaw cycles.

Total RNA was extracted from SC tissue using standardized protocols optimized for neural tissue. RNA concentration and purity were assessed by spectrophotometry, with A260/A280 ratios (**Supplementary Fig. 3**). ranging from 1.9 to 2.0 across all nine samples (n = 1 and n = 8, respectively). RNA integrity was assessed by microfluidic capillary electrophoresis using an Agilent 2100 Bioanalyzer (Agilent Technologies, Santa Clara, CA, USA), which determines the RNA Integrity Number (RIN) from the electrophoretic profile of each sample. All samples met the predefined RNA quality criteria and were subsequently used for microarray analysis. Detailed RNA extraction and quality-control procedures are provided in ***SI Materials and Methods***.

Microarray processing and primary data analysis. High-quality RNA samples were processed for genome-wide expression profiling using Affymetrix Rat Genome 230 2.0 arrays according to the manufacturer's protocols. RNA was reverse-transcribed, amplified, labeled, and hybridized to the arrays, followed by washing, staining, and scanning. Raw fluorescence data were processed using the Microarray Suite 5.0 (MAS 5.0; Affymetrix) algorithm for probe-level background correction and probe-set summarization. Detailed procedures for RNA processing, labeling, hybridization, array processing, scanning, and quality control are provided in ***SI Materials and Methods*.**

Microarray data processing and bioinformatic analysis. To characterize the transcriptional response of SC 24 h after the onset of paralysis, raw Affymetrix Rat Genome 230 2.0 CEL files were independently reprocessed in R using the Bioconductor affy package. Probe-level expression values were summarized using the MAS 5.0 algorithm (Affymetrix), which incorporates perfect-match and mismatch probes and provides probe-set expression estimates together with detection P values. Affymetrix internal control probe sets were excluded from downstream biological analyses, and expression values were log2-transformed MAS 5.0 detection metrics were used as a complementary measure of transcript

detectability in individual samples and were interpreted together with quantitative expression values and biological consistency across replicates.

Probe-set annotation was performed using the rat2302.db, AnnotationDbi, and org.Rn.eg.db Bioconductor packages. Only probe sets that could be unambiguously mapped to an Entrez Gene identifier were retained. When multiple probe sets mapped to the same Entrez Gene identifier, the probe set exhibiting the highest interquartile range across samples was selected to represent the corresponding gene, thereby retaining the probe set with the greatest dynamic range in the experimental dataset.

The resulting expression matrix was analyzed using the Bioconductor limma package. Differential expressions were assessed among control, paralyzed and non-paralyzed animals using linear models, with empirical Bayes moderation applied to stabilize variance estimates across genes. P values were adjusted for multiple testing using the Benjamini–Hochberg procedure. Genes were considered differentially expressed when they met both an adjusted P value ≤0.05 and an absolute log2 fold-change ≥ |1.0|, corresponding to at least a twofold difference in expression. Principal component analysis (PCA) and unsupervised hierarchical clustering were used to assess overall transcriptional relationships among samples and to identify potential sample-level heterogeneity. For visualization, expression values were log2-transformed and, where appropriate, row-wise mean centered. Hierarchical clustering was performed using Pearson correlation as the similarity metric and complete-linkage clustering.

To investigate the biological processes represented by the differentially expressed genes, curated gene sets were assembled based on a focused evaluation of the published literature relevant to ischemic SCI. Functional enrichment analyses were performed in the RStudio environment using Gene Ontology (GO), Kyoto Encyclopedia of Genes and Genomes (KEGG), and Reactome pathway databases. Attention was given to transcriptional programs involved in inflammatory signaling and innate immune activation, monocyte/macrophage recruitment, astrocyte and microglial responses, lipid and DHA metabolism, specialized pro-resolving mediator pathways, neuronal and axonal responses, and extracellular-matrix remodeling. Genes associated with the CCL2/MCP-1 axis, myeloid-cell responses, astrocytic signaling, and lipid mediator biosynthesis were examined in greater detail in relation to the histological, biochemical and functional findings.

Biological pathway and gene-expression analysis. Differentially expressed genes (DEGs) were subjected to functional annotation and pathway-enrichment analyses using Gene Ontology (GO), Kyoto Encyclopedia of Genes and Genomes (KEGG), and Reactome databases. Enrichment analyses were performed using the Enrichr platform and complementary gene-set enrichment approaches, with multiple-testing correction applied to account for multiple comparisons. Pathway-level findings were subsequently integrated with the expression profiles of individual DEGs and with biochemical and histological findings obtained at the corresponding time point. Attention was given to biological processes relevant to acute ischemic SCI, including inflammatory and

innate immune signaling, monocyte/macrophage recruitment, astrocytic and microglial responses, lipid and fatty-acid metabolism, neuronal and axonal responses, and extracellular-matrix remodeling. ***See SI Materials and Methods for details.***

Multiplex cytokine and chemokine analysis. SC tissue was collected separately from the T8, T10, and T12 levels from uninjured controls, MES-stimulated non-paralyzed animals, and MES-stimulated animals with persistent paralysis (n = 3 per group). Cytokine and chemokine concentrations were quantified 24 h after paralysis using a 9-plex SearchLight® protein array (Pierce Biotechnology, Inc., Woburn, MA, USA). Fractalkine, GRO/KC, MCP-1, MIP-2, RANTES, IL-1β, IL-4, IL-6, and TNF-α were measured in SC tissue homogenates. Samples were analyzed in duplicate, and concentrations were calculated from analyte-specific standard curves, adjusted for sample dilution, and expressed as pg/mL. *See* ***SI Materials and Methods*** *for* details.

Magnetic resonance imaging Analysis. MRI was performed on day 5 after MES-induced paralysis at the Gruss Magnetic Resonance Research Center (MRRC), Albert Einstein College of Medicine, Bronx, NY, using a 9.4-T Varian small-animal MRI/MRS system with a 21-cm bore. T2-weighted multislice spin-echo images were acquired for anatomical characterization of the SC. The 9.4-T Varian platform has been used for high-field MRI in experimental rodent models at the Gruss MRRC[20,21]. *See* ***SI Materials and Methods*** *for* details

Morphological, histological and immunohistochemical evidence supporting the transcriptomic finding of an acute spinal cord inflammatory response. To characterize the early tissue response to ischemic SCI, SC segments spanning T8-T12 and encompassing the lesion epicenter were examined. Attention was given to the T10 level, where the lesion was consistently most pronounced. Three animals per group were examined (n = 3 per group).

At 24 h post-paralysis, animals from all three experimental groups were deeply anesthetized and transcardially perfused with 4% paraformaldehyde to ensure tissue collection at a matched post-injury time point across groups. The SC were carefully dissected, post-fixed overnight in 4% paraformaldehyde, and processed for paraffin embedding. Serial coronal sections (10 μm thick) spanning the T8–T12 region were obtained for histological and immunohistochemical evaluation.

Hematoxylin and eosin (H&E) staining was used to assess overall SC architecture and to identify morphological features associated with acute tissue injury, including disruption of tissue organization, cellular accumulation, vacuolization, and areas of altered parenchymal integrity. Consecutive sections encompassing the T8–T12 segment were examined to characterize the spatial distribution of tissue changes relative to the lesion epicenter (T10). Immunohistochemical analyses were performed to characterize cellular responses associated with acute inflammation and gliosis. Astrocytic responses were evaluated using glial fibrillary acidic protein (GFAP), whereas CD11b immunoreactivity was used to identify cells of the myeloid lineage accumulating within the injured SC. Attention was given to the distribution and morphology of CD11b-positive cells, including the appearance of rounded, densely distributed

immunoreactive cells within the injured parenchyma at 24 h after injury. GFAP immunoreactivity was examined to confirm the presence and spatial distribution of astrocytes and the associated gliotic response surrounding the injured tissue. For the purposes of this study, CD11b-positive cells were interpreted as myeloid-lineage cells associated with the inflammatory response and were not classified as microglia or infiltrating macrophages on the basis of morphology or CD11b expression alone. This distinction was considered beyond the scope of the histological analysis in this manuscript and is addressed in the accompanying mechanistic analyses. Detailed quantitative assessment of lesion volume, gliosis, CD11b-positive cell density, and other immunohistochemical endpoints is presented separately in the companion manuscript.

Statistical analysis.

General Statistical Analysis. Quantitative data are presented as mean +/- SD. Lesion volume, Western blotting, and immunohistochemical data were obtained by an investigator blinded to experimental groups. All data were analyzed using Student's t test or one-way ANOVA, where appropriate. All statistical tests were performed using the GraphPad Prism Program, Version 3.02 for Windows (GraphPad Software, San Diego, CA). A P value <0.05 and an α of 0.05 were considered statistically significant.

Ethics Committee

The present study was in strict accordance with the NIH guidelines involving Human Subjects and for Animal welfare assurance and were approved accordingly by Institutional Ethics Committees at Federal University of Rio de Janeiro, Brazil (CAAE 37520820.4.3001.5259 / CEUA UFRJ DAHEICB 053); Hospital Municipal Miguel Couto (CAAE 96263418.0.0000.5279); Brazil; New York Medical College (IACUC approval #69-12-0609.1), NY, and Albert Einstein College of Medicine (IACUC approval protocol #A3312-01; 20030906), NY.

Role of the funding source

The sponsors of this study had no role in study design, data collection, data analysis, data interpretation, or writing of the report. C. M. Perret, T.G. de Morais, and R. Rozental had full access to all the data in the study, and all authors had final responsibility for the decision to submit for publication.

Ethics declarations

All authors declare that they have no conflicts of interest.

RESULTS

Our back-to-back presentation of this study first establishes and characterizes an anesthesia-free model of ischemic SCI induced by repeated MES in awake rats. We first define the reproducibility and neurological phenotype of the model, followed by characterization of lesion anatomy and spatial distribution, the associated astrocytic and myeloid cellular responses, and the transcriptional landscape of the injured SC at 24 h, a critical early time point in the evolution of secondary injury. Detailed quantitative assessments of tissue preservation and lesion volume, together with treatment-dependent changes in GFAP-positive

gliosis, CD11b-positive myeloid-cell responses, additional immunohistochemical endpoints, and functional preservation of the ischemic SC through day 5 after paralysis, are presented separately as complementary analyses in the companion study.

Animal model of repeated MES-induced ischemic SCI. We adapted established transauricular maximal electroshock seizure (MES) paradigms described by Isaac and Advokat[16,17] and subsequently reviewed by Velíšek[18] by modifying the stimulation schedule and including pregnant rats as an experimental cohort. Repeated MES stimulation under these conditions was associated with persistent bilateral hindlimb paralysis and a reproducible thoracic SCI phenotype. Unlike the transient motor impairment reported in previous MES paradigms, the neurological deficits observed here persisted beyond the postictal period and were accompanied by imaging and histopathological evidence of SCI. The resulting phenotype reproduced key neurological and pathological characteristics of ischemic SCI, providing an experimental model for investigating early mechanisms of lesion progression in patients.

The repeated maximal electroshock stimulation (MES) paradigm reliably elicited robust generalized tonic extension of the forelimbs and hindlimbs in all 152 MES-stimulated animals**,** comprising 140 pregnant and 12 age-matched non-pregnant rats**.** Each suprathreshold stimulus produced a consistent behavioral sequence characterized by tonic extension, followed by tonic hindlimb flexion and postictal depression. With repeated stimulation and progression of the protocol, spontaneous flexor and extensor limb contractions, accompanied by pedalling movements, emerged during the interictal periods between stimulation-induced seizures. The pregnant cohort (n = 140) constituted the primary group for assessing the incidence and development of seizure-induced ischemic SCI, whereas the non-pregnant cohort (n = 12) was included as an age-matched comparison group to assess the contribution of pregnancy-associated physiological adaptations.

A constant-voltage stimulus was used to reproduce the classical transauricular MES paradigm originally described by Isaac and Advokat[16]. Across the measured range of transauricular impedances, which remained within previously reported values[19], the applied stimulation generated currents of 90–137 mA and consistently produced generalized seizures with complete tonic hindlimb extension, demonstrating reproducible seizure induction throughout the experimental protocol. *See **SI Materials and Methods** for details.*

Neurological phenotype following repeated MES stimulation. Repeated MES stimulation produced a reproducible neurological phenotype characterized by profound bilateral hindlimb motor impairment and selective sensory deficits below the T10 lesion level (**Fig. 1B**). Of the 140 pregnant animals subjected to the MES protocol, 40 developed hindlimb paralysis; 39 exhibited persistent motor deficits, whereas one recovered hindlimb movements within 3 h of the final stimulation. Thus, persistent paralysis was observed in 39 of 40 animals (97.5%) that initially developed paralysis, consistent with a stable neurological phenotype associated with subsequent ischemic SCI. In these 39 animals, no responses to noxious mechanical pinch applied to the hindlimbs or trunk caudal to the lesion were

detected, indicating severe impairment of nociceptive sensory transmission at these levels. In contrast, noxious stimulation of the tail elicited a localized tail-withdrawal or tail-flick response in 24 of 39 animals (61.5%), indicating preservation of caudal segmental reflex activity. These responses were not accompanied by behavioral signs of supraspinal nociceptive processing, including vocalization, orientation of the head toward the stimulus, escape behavior, attempts to bite the forceps, or generalized body movements. The preservation of segmental tail reflexes despite the absence of detectable nociceptive responses in the hindlimbs and trunk therefore indicates dissociation between caudal spinal reflex activity and ascending sensory transmission. This neurological phenotype remained stable throughout the 5-day observation period following paralysis. Pregnant control animals (n = 20) subjected to the same handling and electrode placement but receiving subthreshold stimulation did not develop seizures or paralysis at any point during the protocol. Importantly, MES-stimulated pregnant animals that developed paralysis did not exhibit premature delivery.

In contrast, repeated MES stimulation in the age-matched non-pregnant group (n = 12) produced transient partial hindlimb paralysis in 2 animals (16.7%). Both animals retained hindlimb movements and responded to noxious mechanical stimulation applied to the trunk caudal to the lesion, and complete neurological recovery occurred within 1 h. Thus, persistent bilateral hindlimb paralysis with associated sensory deficits was observed predominantly in the pregnant cohort, whereas MES stimulation in age-matched non-pregnant animals resulted only in transient and incomplete motor impairment.

Anatomical and cellular characterization of ischemic spinal cord injury

Gross examination of SC specimens revealed distinct macroscopic abnormalities in the 39 animals with persistent paralysis. Lesions were centered predominantly around the T10 SC level, with focal hemorrhagic areas evident at 1 day after paralysis, followed by progressive tissue pallor and atrophy that became more pronounced by day 5 (**Supplementary Fig. 1B)**. In contrast, SC from MES-stimulated non-paralyzed pregnant animals (n = 100), age-matched non-pregnant animals (n = 12), and subthreshold-stimulated pregnant controls (n = 20) showed grossly preserved tissue architecture, without evident focal hemorrhagic abnormalities or areas of tissue vacuolization.

Notably, only approximately 28% of MES-stimulated pregnant animals developed persistent paralysis and the associated SC pathology, despite all animals exhibiting robust tonic hindlimb extension followed by interictal limb contractions. X-ray radiographies did not indicate spinal fracture (**Supplementary Fig. 1C**). The occurrence of SCI in only a subset of similarly stimulated animals argues against mechanical tissue damage resulting from tonic extension or subsequent limb contractions as the primary mechanism of injury.

Consistent with the macroscopic findings, axial T2-weighted MRI demonstrated a characteristic bilateral ventral horn hyperintensity producing an “owl’s-eye”

appearance at the lesion epicenter (**Fig. 1C**), closely resembling the imaging pattern of anterior spinal artery infarction observed clinically (**Fig. 1D**). The abnormal signal extended longitudinally beyond the lesion epicenter, indicating that the injury was not confined to a single SC segment.

Histopathological examination of SC tissue from four randomly selected paralyzed animals independently corroborated the ischemic nature of the lesion (**Fig. 1 E, G, I, K**). Tissue injury was characterized by prominent central necrosis extending into the surrounding white matter, vacuolar degeneration, focal hemorrhage, inflammatory cellular infiltration, and tissue atrophy centered around T10. In sagittal sections, the rostrocaudal extent of injury exceeded one vertebral body in three of four animals examined. In transverse sections, injury frequently involved most of the SC cross-sectional area, whereas the posterior columns were relatively preserved. Histological examination further demonstrated preferential involvement of the anterior two-thirds of the thoracic SC, consistent with the anterior-predominant distribution observed on MRI. Together with the characteristic neurological phenotype and macroscopic evolution, these findings support an anterior spinal artery syndrome-like ischemic lesion rather than a complete transverse SCI.

To define the cellular response within the anatomically characterized lesion, consecutive SC sections spanning T8–T12 were examined, with particular attention to the T10 lesion epicenter. In control SC, GFAP immunoreactivity delineated astrocytes with an organized distribution and characteristic parenchymal morphology (**Fig. 2C–E**). In contrast, injured SC exhibited prominent astrocytic and myeloid responses within and surrounding the affected region. CD11b immunoreactivity revealed a marked increase in myeloid-lineage cells at 24 h after paralysis, with CD11b-positive cells exhibiting predominantly rounded morphologies within the injured parenchyma (**Fig. 2F–H**). This response was accompanied by prominent GFAP-positive astrocytic reactivity surrounding the lesion. The spatial concordance of these responses with the T10-centered lesion provided cellular evidence of an active inflammatory and glial response during the acute phase of ischemic SCI.

Because CD11b is expressed by multiple myeloid populations, CD11b-positive cells were considered collectively as myeloid-lineage cells and were not classified as resident microglia or infiltrating macrophages on the basis of CD11b immunoreactivity or morphology alone. This distinction is particularly relevant to the interpretation of the subsequent bulk-tissue transcriptomic analysis, in which gene-expression profiles represent the composite cellular response of the injured SC and cannot independently resolve cellular origin.

Complementary transcriptomic analyses performed in additional paralyzed animals demonstrated that molecular signatures of inflammatory activation extended caudally below T9 at 24 h after paralysis (**Supplementary Figs. 2B and 4C**). Thus, imaging, histopathology, cellular analysis, and transcriptomic profiling independently converged on an extensive, anterior-predominant ischemic lesion centered around T10, accompanied by persistent perilesional inflammatory activity extending beyond the primary lesion epicenter. Thus, the present study defines the early molecular response at 24 h, whereas the

companion study provides complementary evidence for the subsequent persistence and functional relevance of selected pathways.

These findings establish the anatomical and cellular context for the subsequent 24-h transcriptomic analysis, demonstrating that ischemic SCI is associated with early astrocytic reactivity and myeloid-lineage accumulation within an anterior-predominant lesion. Detailed quantitative analyses of lesion volume, tissue preservation, GFAP-positive gliosis, CD11b-positive cell density, and additional immunohistochemical endpoints are presented in the companion manuscript.

Regional inflammatory response at 24 h after paralysis

Targeted cytokine and chemokine profiling reveals a selective inflammatory response. To characterize the early inflammatory response associated with paralysis, concentrations of nine cytokines and chemokines were quantified in spinal cord (SC) tissue lysates collected 24 h after paralysis using a multiplex 9-plex SearchLight cytokine protein array (**Supplementary Fig. 2**). Inflammatory mediator abundance varied across the lesion-containing segments, with the most pronounced changes detected at the injury epicenter (T10), whereas the more rostral T8 segment showed comparatively fewer alterations (**Supplementary Fig. 2B**). Thus, the early inflammatory response was spatially heterogeneous, with the greatest changes localized to SC regions corresponding to the ischemic lesion.

MCP-1/CCL2 was markedly increased at 24 h, identifying activation of a chemokine axis strongly associated with recruitment of circulating monocytes and macrophages to injured tissue. In contrast, several canonical inflammatory mediators did not exhibit an early increase. TNF-α and IL-6 remained without significant elevation, as did GRO/KC, MIP-2 and IL-1β, fractalkine/CX3CL1 and RANTES/CCL5 although IL-4 was significantly reduced in the injured tissue (**Supplementary Fig. 2F**).

Thus, the acute inflammatory response was not characterized by a generalized increase in inflammatory mediators but rather by a selective and heterogeneous pattern of immune activation in which transcriptional changes did not uniformly translate into corresponding changes in protein abundance. The most prominent concordant response involved the CCL2/MCP-1 axis: MCP-1 protein was markedly increased at 24 h after paralysis, in parallel with robust transcriptional activation of its corresponding gene, *Ccl2*, which exhibited a 117-fold increase in expression by microarray analysis. In contrast, several other inflammatory mediators showed discordant transcript–protein responses. Although *Tnf* transcript expression increased approximately 18-fold at 24 h, TNF-α protein levels were decreased relative to control tissue. Similarly, protein levels of RANTES/CCL5 and IL-4 were reduced, despite the broader transcriptional activation of inflammatory and myeloid-associated programs detected by microarray analysis. These findings indicate that the early response to ischemic SCI was not characterized by a generalized amplification of inflammatory mediator production. Rather, transcriptional activation was selectively translated into protein-level responses, with particularly strong engagement of the CCL2/MCP-1 chemotactic axis, whereas other inflammatory pathways were

attenuated or uncoupled at the protein level. This transcript–protein discordance suggests that post-transcriptional regulation, differences in mediator synthesis and release, protein turnover, and the cellular composition of the injured SC may contribute to shaping the early inflammatory milieu.

Genome-wide transcriptional response at 24 h after paralysis

Transcriptomic profiling identifies a distinct transcriptional response associated with paralysis. Genome-wide analysis of SC tissue collected 24 h after paralysis revealed a distinct transcriptional profile in paralyzed animals compared with both unstimulated controls and MES-stimulated animals that did not develop paralysis (**Figs. 2 and 3**). Paralyzed animals differed from unstimulated controls by 3,720 differentially expressed genes (DEGs) by multiple comparison following FDR selection, including both up- and downregulated transcripts. A comparable but slightly larger transcriptional difference was observed between paralyzed and MES-stimulated non-paralyzed animals, with 4,278 DEGs identified between these groups. Notably, the MES-stimulated non-paralyzed group differed from unstimulated controls by only 3 DEGs, supporting that seizure per se induced by MES-stimulation protocol does not induce SCI. Thus, although repeated MES exposure itself produced measurable transcriptional changes, the magnitude of the transcriptional response was substantially greater in animals that developed paralysis. The extensive divergence of the paralyzed group from both control groups indicates that the major transcriptional remodeling observed at 24 h was associated with the development of the ischemic SC lesion and its early biological response, rather than representing a nonspecific consequence of MES exposure, motor contractions or seizure-related activity alone.

A coordinated cluster of 47 genes showed highly correlated expression patterns across the analyzed samples (**adjusted $P < 0.05$; Figs. 2 and 3**). This cluster included genes previously associated with the response to SCI, including *Aqp4*, *Cd163*, *Fcgr1a* and *Cd14*, together with additional genes identified in the present analysis. Overall, the transcriptional response was characterized by strong activation of inflammatory and myeloid-associated programs accompanied by suppression of several astrocyte-associated homeostatic genes. The inflammatory signature did not correspond to a purely pro-inflammatory transcriptional state. Instead, genes associated with inflammatory activation, immune-cell recruitment and tissue remodeling were expressed concurrently with genes associated with regulation, repair and resolution. This mixed transcriptional phenotype was evident at the 24-h time point and suggested that inflammatory activation and counter-regulatory programs were operating simultaneously during the early response to ischemic SCI.

Myeloid activation and astrocytic transcriptional remodeling

Coordinated myeloid activation and suppression of astrocyte-associated homeostatic programs. Several transcripts associated with activated myeloid cells were increased after paralysis, including *Cd14*, *Fcgr1a* (CD64), *Cd163*, *Mrc1* and *Mafb* (**Fig. 2A-B**). These changes were accompanied by increased expression of inflammatory and chemokine-associated genes, including *Tnf*, *Il6*, *Il1b*, *Ccl2*, *Ccl3*, *Ccl4*, *Cxcl1*, *Cxcl3*, *Cxcl11*, *Cxcl16*, *Tlr2*, *Tlr4*, *Tlr8*, *Tlr1*, *Ptgs2*,

Mmp9, *Socs3*, *Arg1*, *Tgm2* and *Il1rn*. Several additional regulatory genes, including *Cd200r1*, *Il1r2*, *Il18* and *Il1rn*, were also increased. Conversely, expression of several astrocyte-associated genes was reduced, including *Aqp4*, *Acsbg1*, *Aldh1l1*, *Aldoc* and *Ntsr2* (**Fig. 2A-B**). These changes indicate attenuation of transcriptional programs associated with astrocytic homeostasis and metabolism during the acute phase of injury.

Because the analysis was performed on bulk SC tissue, these cell-associated transcriptional signatures do not establish the cellular origin of individual transcripts. Nevertheless, the concurrent induction of myeloid-associated genes and reduction of astrocyte-associated homeostatic genes provides evidence for coordinated remodeling of these cellular compartments at 24 h after ischemic injury.

Lipid-handling and DHA-associated transcriptional remodeling

Ischemic SCI induces coordinated remodeling of lipid metabolism. In parallel with the inflammatory and myeloid transcriptional response, ischemic SCI induced marked remodeling of genes involved in fatty-acid uptake, intracellular lipid storage, and polyunsaturated fatty-acid metabolism (**Fig. 3**). Transcripts associated with fatty-acid uptake and lipid-droplet formation, including *Cd36* (~10-fold), *Plin2* (~24-fold), and *Plin3* (~3.5-fold), were markedly increased. In contrast, transcripts involved in DHA transport and PUFA metabolism were reduced, including *Mfsd2a* (~2.1-fold decrease), *Elovl2* (~6.4-fold decrease), *Elovl4* (~7.3-fold decrease), *Lpcat4* (~4.7-fold decrease), and *Acsl6* (~27-fold decrease). *Faah* expression was also decreased 2.3 fold, indicating concomitant remodeling of fatty-acid amide metabolism. Collectively, these changes revealed a reciprocal lipid-handling signature characterized by increased fatty-acid uptake and intracellular lipid storage together with reduced expression of genes involved in DHA transport, PUFA elongation, phospholipid remodeling, and fatty-acyl activation. This coordinated transcriptional remodeling occurred concomitantly with the early inflammatory response, providing a transcriptional basis for subsequent examination of 17S-H(p)-DHA and related specialized pro-resolving lipid mediators.

ALOX15 activation and validation at the transcript and protein levels. Among genes associated with lipid mediator biosynthesis, *Alox15* was significantly increased in SC tissue 24 h after paralysis. Because 12/15-lipoxygenases catalyze the oxygenation of polyunsaturated fatty acids, including DHA, this finding identified the 12/15-LOX pathway as a potential contributor to DHA-derived lipid mediator metabolism after ischemic SCI.

The transcriptomic finding was independently validated by quantitative RT–PCR. At the injury epicenter, *Alox15* mRNA increased approximately fourfold at 12 h after paralysis following normalization to *Ubc* ($P < 0.05$) (**Supplementary Fig. 4A – *lesion 2***), followed by reduced expression at 24 h (**Supplementary Fig. 4A – *lesion 1*),** indicating a transient transcriptional response to ischemic injury. We next examined whether a similar response could be reproduced under ischemic-like conditions in a defined cellular model. Primary rat SC astrocytes subjected to oxygen–glucose deprivation (OGD) showed a rapid increase in *Alox15* mRNA,

reaching approximately fourfold above normoxic controls during the first 3 h of OGD ($P < 0.01$). Transcript levels subsequently declined toward baseline by 24 h (**Supplementary Fig. 4B**), supporting a transient *Alox15* response to metabolic stress.

At the protein level, Western blotting demonstrated increased 12/15-lipoxygenase (12/15-LOX) abundance in SC tissue from paralyzed animals, reaching approximately sixfold above control levels by day 5 after paralysis ($P < 0.05$; **Supplementary Figs. 4C, 4D**). A predominant immunoreactive band of approximately 75 kDa was detected throughout the lesion-containing T8–T12 region, consistent with the reported molecular mass of ALOX15 and previous detection of a single approximately 75-kDa 12/15-LOX band in rat CNS tissue. Thus, *Alox15* transcription was transiently induced during the early response to ischemic or metabolic stress, whereas 12/15-LOX protein abundance increased at a later stage after injury.

Because 12/15-LOX oxygenates DHA to generate 17-hydroperoxy-DHA, a precursor of 17(S)-HDHA and downstream D-series specialized pro-resolving mediators, increased 12/15-LOX abundance may amplify formation of 15-LOX DHA products following ischemic SCI. The corresponding lipidomic findings are presented in the companion manuscript.

DISCUSSION

In the present study, we establish an anesthesia-free model of ischemic SCI that reproduces key clinical, radiological, histopathological, and molecular features of human condition while enabling high-temporal-resolution analysis of the earliest response to injury. By providing direct access to the first 24 h after paralysis - a critical but incompletely characterized period in which secondary injury processes are initiated - this model reveals that acute ischemic SCI is characterized not simply by excessive inflammation, but by an early disruption of coordinated inflammatory resolution. The initial response was marked by rapid MCP-1/CCL2-associated recruitment of circulating monocytes, heterogeneous macrophage activation, suppression of astrocytic homeostatic programs, and impaired engagement of endogenous lipid-mediated pro-resolving pathways. Together, these findings identify defective inflammatory resolution as a potentially important determinant of early secondary tissue injury after ischemic SCI and provide a mechanistic framework for investigating resolution-based therapeutic strategies.

These observations should be interpreted in the context of limitations inherent to conventional experimental SCI paradigms. A wide range of models - including contusion, compression, transection, crush, and ischemic injury - has provided substantial mechanistic insight into SCI pathophysiology, while differing substantially in injury mechanism, tissue biomechanics, anatomical distribution, and translational relevance[22,23]. Most traumatic SCI paradigms require surgical exposure of the SC and are performed under general anesthesia, introducing physiological variables that are not intrinsic to the injury itself. Anesthesia and the associated perioperative state can alter autonomic and cardiovascular function and modulate neuroendocrine and immune responses, including cytokine production, leukocyte trafficking, and inflammatory-cell function[24,25]. These

effects are particularly relevant when investigating the earliest molecular and cellular responses to injury, because anesthetic exposure may modify the temporal and magnitude of inflammatory signaling independently of the primary lesion. Biomechanical characteristics represent an additional source of experimental variability. Conventional weight-drop and contusion paradigms depend on parameters such as impact force, displacement, velocity, and tissue deformation, which can influence lesion severity and functional outcome. The development of force-controlled devices has specifically sought to reduce variability associated with tissue movement and injury mechanics[26,27]. Nevertheless, even standardized contusion models produce graded and spatially heterogeneous lesions, emphasizing the importance of precise control and characterization of the primary insult. Collectively, differences in injury mechanism, anesthesia, perioperative physiology, and biomechanical control may influence the acute neurovascular and inflammatory environment and complicate comparisons across experimental paradigms. Such factors may contribute to the difficulty of translating promising preclinical findings into effective clinical interventions, as illustrated by the limited clinical success of pharmacological interventions in acute SCI[28].

Within this framework, the thoracolumbar SC represents a region of intrinsic vascular vulnerability because of its dependence on a limited and variable radiculomedullary arterial supply. In humans, perfusion of the lower thoracic cord by the anterior spinal artery is commonly reinforced by the artery of Adamkiewicz, whereas in rats it depends on multiple segmental feeders with species-specific patterns and substantial inter-individual variability[29–31]. This vascular organization may limit perfusion reserve during systemic hemodynamic disturbances, potentially rendering thoracic segments susceptible to transient hypoperfusion[32,33]. Generalized tonic seizures constitute a substantial systemic perturbation, associated with hypoxia, autonomic instability and fluctuations in cardiovascular function[34]. Consistent with the possibility of transient hypoperfusion and reversible conduction failure, a subset of non-pregnant animals developed transient paralysis following electroconvulsive stimulation, resembling transient postictal neurological deficits described clinically[35].

In contrast, animals that developed persistent paralysis exhibited bilateral ventral horn hyperintensities with the characteristic “owl’s-eye” appearance on MRI, a pattern strongly associated with ischemic SCI. The distinction between ischemic injury and stimulation-related mechanical effects was further supported by the transcriptomic data. Paralyzed animals exhibited 3,720 DEGs compared with unstimulated controls and 4,278 DEGs compared with MES-stimulated non-paralyzed animals, whereas MES-stimulated non-paralyzed animals differed from unstimulated controls by only 3 DEGs following FDR correction. Thus, exposure to MES, seizures and the associated muscle contractions produced minimal transcriptional perturbation in animals that remained neurologically intact, whereas persistent paralysis was accompanied by a distinct molecular response. Together with the characteristic MRI phenotype, these findings support an ischemic rather than mechanically traumatic origin of the persistent SC lesion.

Irreversible paralysis occurred exclusively in pregnant animals subjected to repeated MES stimulation, indicating that pregnancy may represent a critical

permissive factor for sustained SC ischemia. The higher incidence during the second week of gestation suggests a temporally restricted period of increased vulnerability, potentially reflecting redistribution of systemic blood flow toward the uteroplacental circulation and a consequent reduction in SC perfusion reserve. Under these conditions, seizure-associated hypoxia and hemodynamic instability may precipitate sustained hypoperfusion within vulnerable thoracolumbar segments, ultimately exceeding the threshold for irreversible tissue injury. The incidence of permanent paralysis may also reflect inter-individual differences in radiculomedullary vascular reinforcement in rats[29], further suggesting that anatomical variation in SC perfusion contributes to susceptibility to systemic ischemic stress.

A distinctive feature of the neurological phenotype was the dissociation between loss of nociceptive responses below the lesion and preservation of a localized tail-withdrawal response. Paralyzed animals consistently failed to respond to noxious stimulation of the hindlimbs and trunk caudal to the lesion, with no accompanying vocalization, head orientation, escape behavior or generalized movements. This finding is consistent with substantial disruption of ascending nociceptive pathways traversing the thoracic cord, particularly the anterolateral system, while sparing more caudal segmental circuitry. In contrast, tail pinch elicited a localized withdrawal or flick response in a subset of animals, most likely reflecting preservation of sacral and coccygeal spinal reflex circuits located caudal to the thoracic lesion. Importantly, these responses occurred without behavioral evidence of supraspinal nociceptive processing, supporting their interpretation as segmental spinal reflexes rather than evidence of preserved conscious nociception.

In patients, SC ischemia produces an evolving lesion in which neurological deficits are followed by progressive radiographic changes, including SC swelling, T2-weighted signal abnormalities and, in some cases, contrast enhancement. Serial MRI studies indicate that abnormalities may be subtle or absent during the first hours after symptom onset and become more apparent over the subsequent 24–72 h, consistent with an evolving secondary injury process rather than a static ischemic insult[36,37]. Ischemia, vascular dysfunction, blood–spinal cord barrier disruption, edema, excitotoxicity and inflammatory signaling interact during this period, with recruitment of circulating leukocytes and activation of resident glial cells contributing to lesion progression[1,38]. Among these responses, the CCL2/MCP-1–CCR2 axis is particularly important for early recruitment of circulating monocytes to injured SC tissue[4,39]. Monocyte-derived macrophages subsequently accumulate within the lesion and participate in clearance of myelin and cellular debris, whereas resident microglia exhibit temporally and spatially distinct responses[40]. Human pathological studies similarly demonstrate spatial segregation of these populations during lesion maturation, with TMEM119-negative blood-derived macrophages becoming prominent within the lesion core and TMEM119-positive resident microglia remaining more evident at the lesion rim[41].

The temporal and cellular pattern observed in our model is consistent with this evolving inflammatory response. At 24 h, functional deficits were accompanied by disruption of SC architecture at the lesion epicenter, including tissue contour

distortion, reduced tissue volume, heterotopically nucleated cells compatible with mononuclear phagocyte accumulation, and features consistent with early edema. Semi-quantitative analysis demonstrated a marked increase in CD11b-positive perilesional areas, indicating substantial myeloid-cell accumulation. Because CD11b is expressed by both resident microglia and infiltrating macrophages, this marker alone cannot establish cellular origin. However, the absence of a detectable change in *Tmem119* expression, together with the increased expression of macrophage-associated genes, supports a greater contribution of recruited monocyte-derived myeloid cells to the early CD11b-positive response, while acknowledging that definitive discrimination between microglia and infiltrating macrophages would require lineage-specific markers or fate-mapping approaches[39–41]. Over the subsequent 3–5 days, vacuolar degeneration and tissue disruption became more pronounced, accompanied by increasing organization of the tissue surrounding the lesion, consistent with evolving reactive gliosis and early remodeling. Thus, the model captures temporal progression from early myeloid accumulation and tissue disruption to progressive structural degeneration and gliotic remodeling.

A prominent feature of the 24-h transcriptional profile was coordinated alteration of genes involved in lipid uptake, storage and polyunsaturated fatty-acid metabolism. *Plin2*, *Plin3* and *Cd36* were upregulated, whereas genes involved in fatty-acid transport and polyunsaturated fatty-acid metabolism, including *Mfsd2a*, *Fads1*, *Fads2* and *Elovl4*, were reduced. This pattern suggests increased lipid uptake and intracellular sequestration occurring alongside reduced capacity for lipid transport, elongation, desaturation and membrane lipid remodeling. Such metabolic reprogramming can accompany activation of macrophages and other myeloid cells, in which altered lipid handling influences inflammatory signaling, cellular phenotype and tissue repair[14,42]. The concurrent induction of lipid-storage genes and suppression of polyunsaturated fatty-acid metabolic pathways therefore suggests that ischemic injury induces not only an inflammatory response but also a substantial metabolic reorganization of the injured SC. Importantly, these findings should not be interpreted as evidence that lipid accumulation itself represents a macrophage-specific phenomenon, because the analysis was performed on bulk SC tissue. Rather, they identify a tissue-level metabolic state occurring in parallel with the recruitment and activation of myeloid cells. Such remodeling may favor intracellular lipid accumulation while restricting polyunsaturated fatty-acid availability and membrane lipid renewal, potentially contributing to persistence of inflammatory signaling and limiting the transition toward resolution. This interpretation is consistent with the broader concept that resolution of inflammation is an active, metabolically regulated process, rather than simply the passive disappearance of inflammatory signals[14,42]. The specific consequences of this altered lipid environment for DHA-derived pro-resolving pathways are addressed in the companion study.

Within this altered metabolic landscape, astrocytes and macrophage-lineage cells emerge as functionally divergent components of the early response to ischemic SCI**.** Astrocytic transcriptional programs were markedly suppressed within the first 24 h after injury, including reduced expression of genes involved in metabolic and homeostatic functions and, notably, *Aqp4*. AQP4 is enriched in astrocytic perivascular endfeet and contributes to perivascular CSF–interstitial

fluid exchange and extracellular solute clearance[43]. Thus, reduced *Aqp4* expression may indicate early disruption of an astrocytic perivascular fluid-clearance/glymphatic-like mechanism, potentially compromising extracellular fluid and metabolic homeostasis after ischemic SCI. Such dysfunction could also influence the local persistence or clearance of inflammatory mediators, including MCP-1, although this relationship was not directly tested. Thus, suppression of astrocytic homeostatic programs occurred concurrently with activation and accumulation of myeloid cells, suggesting an early imbalance between inflammatory recruitment and tissue-supportive mechanisms.

Direct transcriptomic analyses of human ischemic SC tissue remain rare because acute clinical specimens are difficult to obtain. Nevertheless, human SCI transcriptomic and biomarker studies identify inflammatory, chemokine, macrophage-associated and glial pathways that overlap with the molecular programs observed here. In our model, inflammatory and myeloid-associated transcripts - including *Tnf*, *Il1b*, *Il6*, *Alox5ap* and *Ccl2/Mcp-1*- were altered at 24 h, whereas protein analysis showed a pronounced increase predominantly in MCP-1/CCL2, with several canonical cytokines and chemokines remaining unchanged or reduced. This apparent transcript–protein divergence may reflect the dynamic nature of the acute ischemic response, in which transcriptional activation can precede translation, processing, secretion or extracellular accumulation. Ischemia-associated metabolic dysfunction, oxidative stress and translational suppression may further contribute to this temporal dissociation. These findings support a model in which the inflammatory response to SCI is temporally and molecularly selective rather than a uniform cytokine surge. Hellenbrand et al. [44] demonstrated that individual inflammatory mediators exhibit distinct kinetics after SCI, with some showing early transient induction but largely returned toward uninjured levels by ~24h, whereas others remain elevated at later stages. Consistent with this temporal framework, we detected no significant increase in IL-6 at 24 h, whereas Sabirov et al.[45] reported a marked increase in CSF IL-6 approximately 3 days after human SCI followed by a subsequent decline. Differences in individual mediator levels between studies may therefore reflect sampling time, biological compartment and injury phase rather than fundamental differences in inflammatory biology.

The clinical relevance of MCP-1 is further supported by studies identifying this chemokine as an important component of the acute human SCI response[46] and associating its levels with injury severity and outcome[47]. The predominance of *Ccl2/Mcp-1* signaling in the 24-h SC response observed here therefore parallels the early CSF biomarker response described clinically, supporting the biological relevance of chemokine-dependent myeloid recruitment in acute SCI. In conjunction with the CD11b and *Tmem119* findings, these data suggest that the early inflammatory response is characterized primarily by recruitment and activation of circulating myeloid cells rather than synchronous activation of all canonical inflammatory cytokines.

The macrophage response itself did not conform to a simple M1/M2 dichotomy. Increased expression of macrophage-associated genes occurred alongside relatively modest protein-level induction of canonical inflammatory mediators and reductions in IL-4 and RANTES. These findings support a heterogeneous

activation state rather than discrete pro-inflammatory or reparative polarization during the first 24 h. Previous studies similarly indicate that macrophage responses within injured SC tissue are temporally and phenotypically heterogeneous and cannot be fully captured by a binary M1/M2 classification[48]. The coexistence of early myeloid recruitment with suppression of astrocytic homeostatic programs suggests that inflammatory activation develops within a tissue environment in which mechanisms required for containment and resolution are simultaneously compromised.

Importantly, several features of the molecular response identified here overlap with those described after traumatic SCI, including MCP-1-associated monocyte recruitment, astrocytic dysfunction and altered inflammatory and lipid signaling. Such convergence suggests that ischemic and traumatic SCI may engage shared secondary injury pathways despite differences in the initiating insult. The anesthesia-free nature of the present model provides an additional experimental advantage by minimizing potential suppression of neuroimmune responses and permitting investigation of early molecular events without surgical exposure. This is particularly relevant during the first 24 h, when secondary injury mechanisms may remain amenable to intervention. Collectively, our findings support a model in which early ischemic SCI is governed by the interaction of vascular compromise, selective myeloid recruitment, astrocytic homeostatic dysfunction and metabolic remodeling. Rather than representing an indiscriminate inflammatory surge, the acute response appears to involve a mismatch between rapid recruitment of inflammatory cells and insufficient engagement of mechanisms required for effective resolution. This framework suggests that therapeutic strategies directed exclusively at suppressing inflammation may be insufficient and potentially counterproductive if they also inhibit reparative or resolution-associated programs. Approaches that restore tissue homeostasis while selectively modulating inflammatory recruitment may therefore provide a more effective strategy for limiting secondary injury. The companion manuscript addresses the downstream consequences of this altered inflammatory–lipid environment and specifically examines endogenous and therapeutic pro-resolving lipid mediator pathways after ischemic SCI.

ACKNOWLEDGMENTS. We thank Dr. L. de Brito Gitirana (ICB/UFRJ) for assistance with histology; Drs R. Mesquita and L. Lima (BioINFO, UFRJ) for assistance with transcriptomic analyses; Dr D. Patel (Genome Explorations, Memphis, TN, USA) for assistance with the microarray assays; and Dr. L. A. Alves (IOC/Fiocruz) for valuable comments. This work was supported in part by Spinal Cord New York State–Spinal Cord Injury Research C022068 (to R.R.), the Fundação Carlos Chagas Filho de Amparo a Pesquisa do Estado do Rio de Janeiro (FAPERJ; E-26/110.625, to R.R.), and grants from the Brazilian Ministry of Health (to R.R.; TED 1302016-UFRJ and VPPIS 00422278-Fiocruz).

COMPETING INTERESTS

The authors declare no competing financial interests in relation to the work described in this manuscript.

Data availability. The microarray gene expression dataset generated in this study has been deposited in the NCBI Gene Expression Omnibus (GEO) under accession number GSE345827

Author contributions

F.A.L. and R.R. developed the animal model. F.A.L., K.G. and R.R. designed the research; T.G.M., C.P., K.G. and R.R. performed the experiments; T.G.M. performed the microarray analysis, and T.G.M., C.P. and K.G. conducted the molecular biological assays. R.R. coordinated the experiments; T.G.M., C.P., K.G. and R.R. analyzed the data; and R.R. wrote the manuscript.

REFERENCES

1. Ahuja, C. S. *et al.* Traumatic spinal cord injury. *Nat. Rev. Dis. Primers* **3**, 17018 (2017).

2. Upton, D. H., Popovic, K., Fulton, R. & Kassiou, M. Anaesthetic-dependent changes in gene expression following acute and chronic exposure in the rodent brain. *Sci. Rep.* **10**, 9366 (2020).

3. Kobayashi, N., Davis, J. A., Phinney, C. T. & Grau, J. W. Regional anesthesia after spinal cord injury attenuates behavioral loss, hemorrhage, and cell death. *Front. Neurol.* **Volume 17-2026**, (2026).

4. Milich, L. M. *et al.* Single-cell analysis of the cellular heterogeneity and interactions in the injured mouse spinal cord. *Journal of Experimental Medicine* **218**, (2021).

5. Hakim, R. *et al.* Spinal cord injury induces permanent reprogramming of microglia into a disease-associated state which contributes to functional recovery. *Journal of Neuroscience* **41**, 8441–8459 (2021).

6. Gensel, J. C., Kopper, T. J., Zhang, B., Orr, M. B. & Bailey, W. M. Predictive screening of M1 and M2 macrophages reveals the immunomodulatory effectiveness of post spinal cord injury azithromycin treatment. *Sci. Rep.* **7**, 40144 (2017).

7. Beck, K. D. *et al.* Quantitative analysis of cellular inflammation after traumatic spinal cord injury: evidence for a multiphasic inflammatory response in the acute to chronic environment. *Brain* **133**, 433–447 (2010).

8. B, B. M. *et al.* A Randomized, Controlled Trial of Methylprednisolone or Naloxone in the Treatment of Acute Spinal-Cord Injury. *New England Journal of Medicine* **322**, 1405–1411 (1990).

9. Fehlings, Michael G *et al.* A Clinical Practice Guideline for the Management of Patients With Acute Spinal Cord Injury and Central Cord Syndrome: Recommendations on the Timing (≤24 Hours Versus >24 Hours) of Decompressive Surgery. *Global Spine J.* **7**, 195S-202S (2017).

10. Valente, M., Dentoni, M., Bellizzi, F., Kuris, F. & Gigli, G. L. Specialized Pro-Resolving Mediators in Neuroinflammation: Overview of Studies and Perspectives of Clinical Applications. *Molecules* **27**, (2022).

11. Bazan, N. G. Neuroprotectin D1-mediated anti-inflammatory and survival signaling in stroke, retinal degenerations, and Alzheimer's disease. *J. Lipid Res.* **50**, S400–S405 (2009).

12. Tiberi, M. & Chiurchiù, V. Specialized Pro-resolving Lipid Mediators and Glial Cells: Emerging Candidates for Brain Homeostasis and Repair. *Front. Cell. Neurosci.* **15**, 673549 (2021).

13. Ren, Y. Z., Zhang, B. Z., Zhao, X. J. & Zhang, Z. Y. Resolvin D1 ameliorates cognitive impairment following traumatic brain injury via protecting astrocytic mitochondria. *J. Neurochem.* **154**, 530–546 (2020).

14. Dalli, J. & Serhan, C. N. Pro-resolving mediators in regulating and conferring macrophage function. *Front. Immunol.* **8**, 296210 (2017).

15. Xu, J. *et al.* CNS and CNS diseases in relation to their immune system. *Front. Immunol.* **Volume 13-2022**, (2022).

16. Isaac, L. & Advokat, C. Reversible motor paralysis in rats after repeated electroconvulsive shock. *Exp. Neurol.* **85**, 87–96 (1984).

17. Isaac, L., Advokat, C., Nelson, D. K. & Browning, R. A. Motor paralysis in rats after repeated electroconvulsive shock: Comparison between aural and corneal stimulation. *Life Sci.* **37**, 1257–1264 (1985).

18. Velíšková, J. & Velíšek, L. Behavioral Characterization and Scoring of Seizures in Rodents. *Models of Seizures and Epilepsy: Second Edition* 111–123 (2017) doi:10.1016/B978-0-12-804066-9.00009-2.

19. Vöröslakos, M. *et al.* Direct effects of transcranial electric stimulation on brain circuits in rats and humans. *Nature Communications 2018 9:1* **9**, 483- (2018).

20. Gomes, W. A. *et al.* Spectroscopic imaging of the pilocarpine model of human epilepsy suggests that early NAA reduction predicts epilepsy. *Magn. Reson. Med.* **58**, 230–235 (2007).

21. Miyasaka, N., Takahashi, K. & Hetherington, H. P. 1H MMR spectroscopic imaging of the mouse brain at 9.4 T. *Journal of Magnetic Resonance Imaging* **24**, 908–913 (2006).

22. Cheriyan, T. *et al.* Spinal cord injury models: a review. *Spinal Cord* **52**, 588–595 (2014).

23. Sharif-Alhoseini, M. *et al.* Animal models of spinal cord injury: a systematic review. *Spinal Cord* **55**, 714–721 (2017).

24. Kurosawa, S. & Kato, M. Anesthetics, immune cells, and immune responses. *J. Anesth.* **22**, 263–277 (2008).

25. Cruz, F. F., Rocco, P. R. M. & Pelosi, P. Anti-inflammatory properties of anesthetic agents. *Critical Care 2017 21:1* **21**, 67- (2017).

26. Gruner, J. A. A monitored contusion model of spinal cord injury in the rat. *J. Neurotrauma* **9**, 123–128 (1992).

27. Scheff, S. W., Rabchevsky, A. G., Fugaccia, I., Main, J. A. & Lumpp, J. E. Experimental modeling of spinal cord injury: characterization of a force-defined injury device. *J. Neurotrauma* **20**, 179–193 (2003).

28. Bracken, M. B. & Holford, T. R. Effects of timing of methylprednisolone or naloxone administration on recovery of segmental and long-tract neurological function in NASCIS 2. *J. Neurosurg.* **79**, 500–507 (1993).

29. Schievink, W. I., Luyendijk, W. & Los, J. A. Does the artery of Adamkiewicz exist in the albino rat? *J. Anat.* **161**, 95 (1988).

30. Tveten, L. Spinal cord vascularity. IV. The spinal cord arteries in the rat. *Acta Radiol. Diagn. (Stockh).* **17**, 385–398 (1976).

31. Mazensky, D., Flesarova, S. & Sulla, I. Arterial Blood Supply to the Spinal Cord in Animal Models of Spinal Cord Injury. A Review. *Anat. Rec. (Hoboken)* **300**, 2091–2106 (2017).

32. Shamji, M. F., Maziak, D. E., Shamji, F. M., Ginsberg, R. J. & Pon, R. Circulation of the spinal cord: An important consideration for thoracic surgeons. *Annals of Thoracic Surgery* **76**, 315–321 (2003).

33. Marsala, M., Sorkin, L. S. & Yaksh, T. L. Transient spinal ischemia in rat: characterization of spinal cord blood flow, extracellular amino acid release, and concurrent histopathological damage. *J. Cereb. Blood Flow Metab.* **14**, 604–614 (1994).

34. Löscher, W. & Schmidt, D. Which animal models should be used in the search for new antiepileptic drugs? A proposal based on experimental and clinical considerations. *Epilepsy Res.* **2**, 145–181 (1988).

35. Selman, B. A., Hassan, M. S., Rahimov, R., Mert, S. & Köksal, A. Todd Paralysis in a Pregnant Mother Presenting as Acute Stroke: Case Report. *Int. Med. Case Rep. J.* **17**, 367–370 (2024).

36. Kim, B. R. *et al.* Features of non-traumatic spinal cord infarction on MRI: Changes over time. *PLoS One* **17**, e0274821 (2022).

37. Zalewski, N. L. *et al.* Characteristics of Spontaneous Spinal Cord Infarction and Proposed Diagnostic Criteria. *JAMA Neurol.* **76**, 56–63 (2019).

38. Anwar, M. A., Al Shehabi, T. S. & Eid, A. H. Inflammogenesis of Secondary Spinal Cord Injury. *Front. Cell. Neurosci.* **10**, 98 (2016).

39. Shechter, R. *et al.* Recruitment of beneficial M2 macrophages to injured spinal cord is orchestrated by remote brain choroid plexus. *Immunity* **38**, 555–569 (2013).

40. Greenhalgh, A. D. *et al.* Peripherally derived macrophages modulate microglial function to reduce inflammation after CNS injury. *PLoS Biol.* **16**, e2005264 (2018).

41. Zrzavy, T. *et al.* Acute and non-resolving inflammation associate with oxidative injury after human spinal cord injury. *Brain* **144**, 144–161 (2021).

42. Serhan, C. N. Pro-resolving lipid mediators are leads for resolution physiology. *Nature 2014 510:7503* **510**, 92–101 (2014).

43. Mestre, H. *et al.* Aquaporin-4-dependent glymphatic solute transport in the rodent brain. *Elife* **7**, (2018).

44. Hellenbrand, D. J. *et al.* The secondary injury cascade after spinal cord injury: an analysis of local cytokine/chemokine regulation. *Neural Regen. Res.* **19**, 1308–1317 (2024).

45. Sabirov, D. *et al.* Comparative Analysis of Cytokine Profiles in Cerebrospinal Fluid and Blood Serum in Patients with Acute and Subacute Spinal Cord Injury. *Biomedicines* **11**, (2023).

46. Tsai, M. C. *et al.* Inflammatory mediators of cerebrospinal fluid from patients with spinal cord injury. *Surg. Neurol.* **70**, S19–S24 (2008).

47. Kwon, B. K. *et al.* Cerebrospinal Fluid Biomarkers To Stratify Injury Severity and Predict Outcome in Human Traumatic Spinal Cord Injury. *J. Neurotrauma* **34**, 567–580 (2017).

48. Stapenhorst França, F. & Gensel, J. C. Redefining macrophage phenotypes after spinal cord injury: An open data approach. *Exp. Neurol.* **388**, 115222 (2025).

MAIN FIGURE LEGENDS

Fig. 1. Overall characterization of the awake MES-induced ischemic spinal cord injury model in rats. (**A**) Representative image during the MES protocol showing a generalized tonic-clonic seizure with robust bilateral extension of the forelimbs and hindlimbs elicited by electrical stimulation. (**B**) Assessment of nociceptive responses following standardized mechanical pinches applied to the hindlimbs, tail, and trunk, demonstrating bilateral hindlimb paralysis and loss of nociceptive sensation below the T10–T12 level; the “black line” indicates the approximate neurological level of sensory impairment. (**C,D**) Representative T2-weighted MRI images of the T10–T12 SC in a paralyzed rat (**C**) and a patient with ischemic SCI (**D**). Enlarged insets show the characteristic bilateral “owl-eyes” pattern associated with ischemic injury in the rat and patient. (**E**) Macroscopic examination at day 5 after paralysis showing a focal ischemic lesion centered at the T10–T12 level (arrow). (**F–K**) Representative H&E-stained transverse SC sections from control (**F,H,J**) and paralyzed (**G,I,K**) animals. Compared with controls, paralyzed animals exhibited marked disruption of normal SC architecture, including loss of gray–white matter organization, distortion of the central canal, tissue rarefaction, and volumetric loss, with prominent alterations extending across the anterior–posterior axis. Magnification: (**F, G**) 10×; (**H, I**) 20×; and (**J, K**) 40×. The scale bar shown in panel **K** applies to all histological panels and corresponds to 400 μm (**F, G),** 200 μm (**H, I)**, and 100 μm (**J, K).**

Fig. 2. Transcriptomic and histological characterization of astrocytic and myeloid responses at 24 h after ischemic spinal cord injury. (**A**) Microarray analysis showed reduced expression of astrocyte-associated genes and increased expression of myeloid/macrophage-associated genes in paralyzed animals compared with uninjured controls and MES-stimulated non-paralyzed animals. (**B**) Schematic representation of selected differentially expressed genes associated with astrocytes and macrophages, highlighting inflammatory and activation/polarization pathways. (**C–E**) Representative SC sections from control animals showing the distribution of $GFAP^+$ astrocytes and resident microglia. (**F–H**) Corresponding sections 24 h after ischemic SCI demonstrating altered astrocytic organization and accumulation of $CD11b^+$ myeloid cells, including activated microglia and infiltrating macrophage-lineage cells. Together, these findings indicate a predominantly $CD11b^+$ myeloid response, whereas astrocytes showed a comparatively minor and secondary transcriptional response. The scale bar shown in panel **H** applies to all histological panels and corresponds to 500 µm (**C, F**), 250 µm (**D, G**), and 100 µm (**E, H**).

Fig. 3. Transcriptomic profiling of macrophage activation and DHA/EPA metabolic pathways at 24 h after ischemic spinal cord injury. (**A,B**) Gene-enrichment analysis identified increased expression of both M1- and M2-associated macrophage gene programs in paralyzed animals compared with uninjured controls and MES-stimulated non-paralyzed animals. The concurrent enrichment of both programs, without a clear separation into a predominant M1 or M2 phenotype, indicates an early and heterogeneous macrophage activation state following ischemic SCI. **(B)** Analysis of DHA/EPA-associated genes revealed increased expression of selected lipid-related and M2-associated markers, together with reduced expression of genes involved in the biosynthesis, uptake, transport, and intracellular retention of polyunsaturated fatty acids required for the generation of specialized pro-resolving mediators (SPMs)**.** These findings suggest that, despite activation of macrophage-associated lipid programs, the injured SC exhibits a transcriptional constraint on the availability and metabolism of DHA/EPA substrates required for effective SPM biosynthesis. (**C**) Schematic representation of selected differentially expressed genes associated with M1- and M2-associated macrophage programs and DHA/EPA metabolism, illustrating their relationships with inflammatory signaling, macrophage activation, lipid handling, and SPM biosynthetic pathways.

Figures

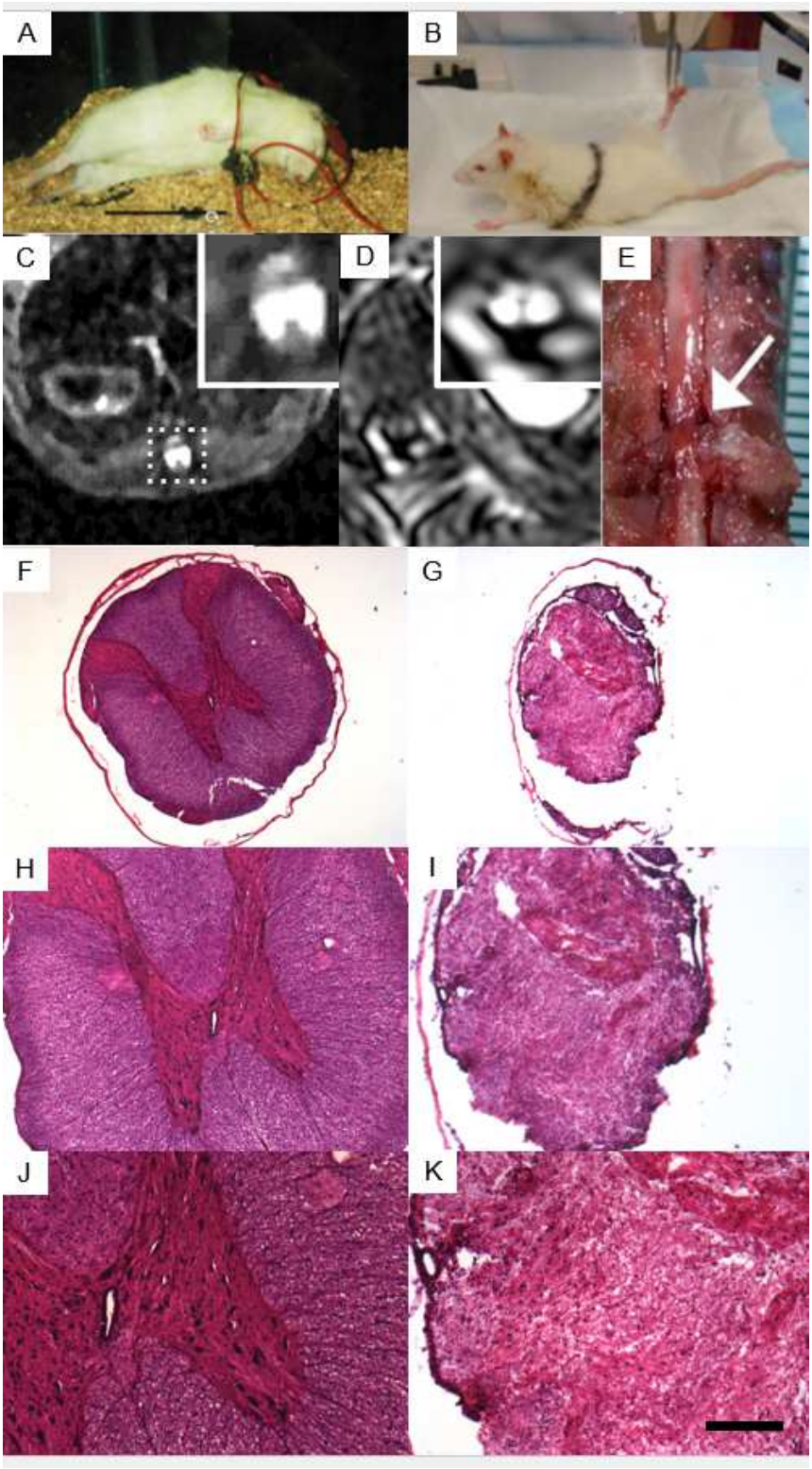


Figure 1

Fig. 1. Overall characterization of the awake MES-induced ischemic spinal cord injury model in rats. (A) Representative image during the MES protocol showing a generalized tonic-clonic seizure with robust bilateral extension of the forelimbs and hindlimbs elicited by electrical stimulation. (B) Assessment of

nociceptive responses following standardized mechanical pinches applied to the hindlimbs, tail, and trunk, demonstrating bilateral hindlimb paralysis and loss of nociceptive sensation below the T10–T12 level; the “black line” indicates the approximate neurological level of sensory impairment. (C,D) Representative T2-weighted MRI images of the T10–T12 SC in a paralyzed rat (C) and a patient with ischemic SCI (D). Enlarged insets show the characteristic bilateral “owl-eyes” pattern associated with ischemic injury in the rat and patient. (E) Macroscopic examination at day 5 after paralysis showing a focal ischemic lesion centered at the T10–T12 level (arrow). (F–K) Representative H&E-stained transverse SC sections from control (F,H,J) and paralyzed (G,I,K) animals. Compared with controls, paralyzed animals exhibited marked disruption of normal SC architecture, including loss of gray–white matter organization, distortion of the central canal, tissue rarefaction, and volumetric loss, with prominent alterations extending across the anterior–posterior axis. Magnification: (F, G) 10×; (H, I) 20×; and (J, K) 40×. The scale bar shown in panel K applies to all histological panels and corresponds to 400 μm (F, G), 200 μm (H, I), and 100 μm (J, K).

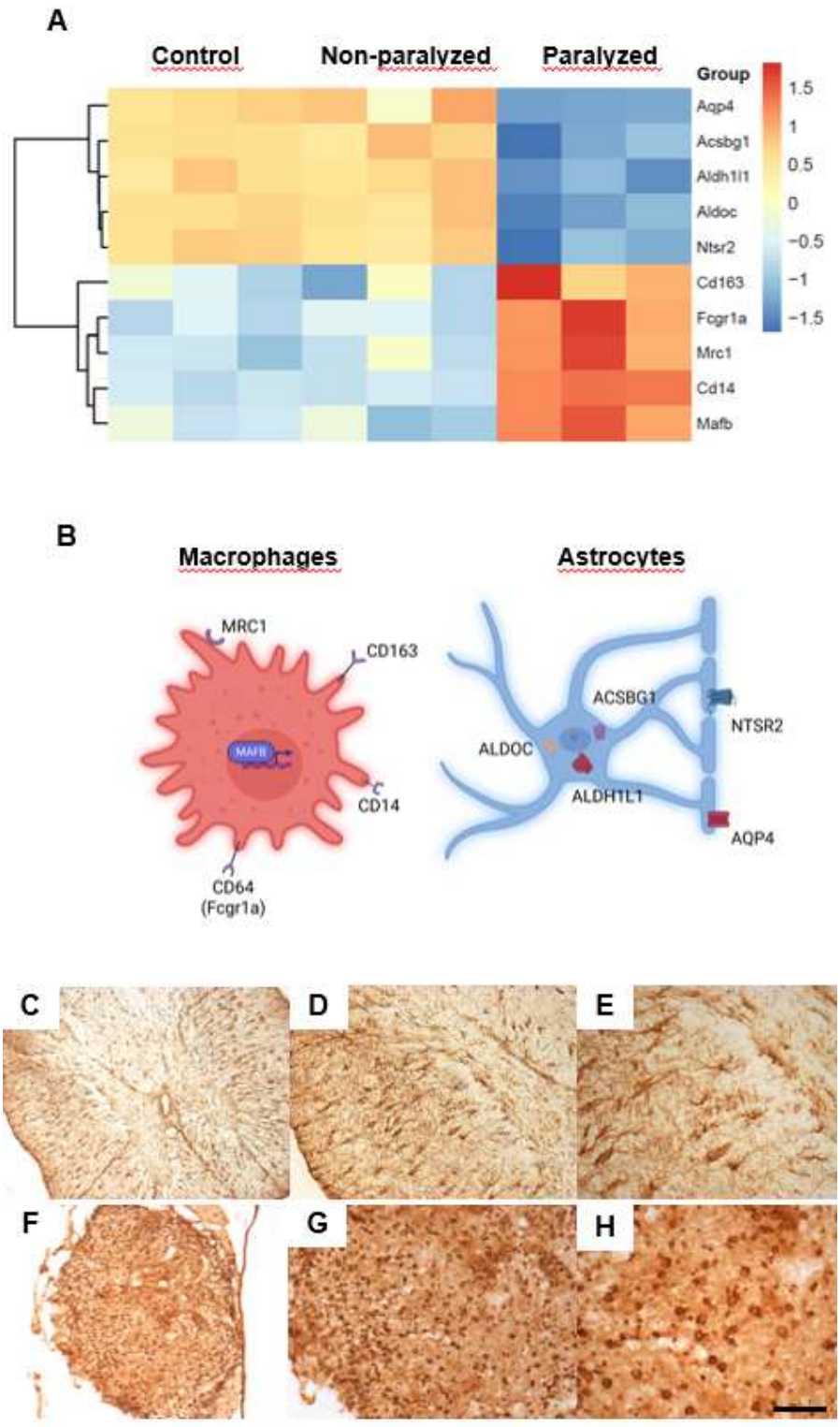


Figure 2

Fig. 2. Transcriptomic and histological characterization of astrocytic and myeloid responses at 24 h after ischemic spinal cord injury. (A) Microarray analysis showed reduced expression of astrocyte-associated genes and increased expression of myeloid/macrophage-associated genes in paralyzed animals compared with uninjured controls and MES-stimulated non-paralyzed animals. (B) Schematic representation of selected differentially expressed genes associated with astrocytes and macrophages,

highlighting inflammatory and activation/polarization pathways. (C–E) Representative SC sections from control animals showing the distribution of GFAP⁺ astrocytes and resident microglia. (F–H) Corresponding sections 24 h after ischemic SCI demonstrating alteredastrocytic organization and accumulation of CD11b⁺ myeloid cells, including activated microglia and infiltrating macrophage-lineage cells. Together, these findings indicate a predominantly CD11b⁺ myeloid response, whereas astrocytes showed a comparatively minor and secondary transcriptional response. The scale bar shown in panel H applies to all histological panels and corresponds to 500 μm (C, F), 250 μm (D, G), and 100 μm (E, H).

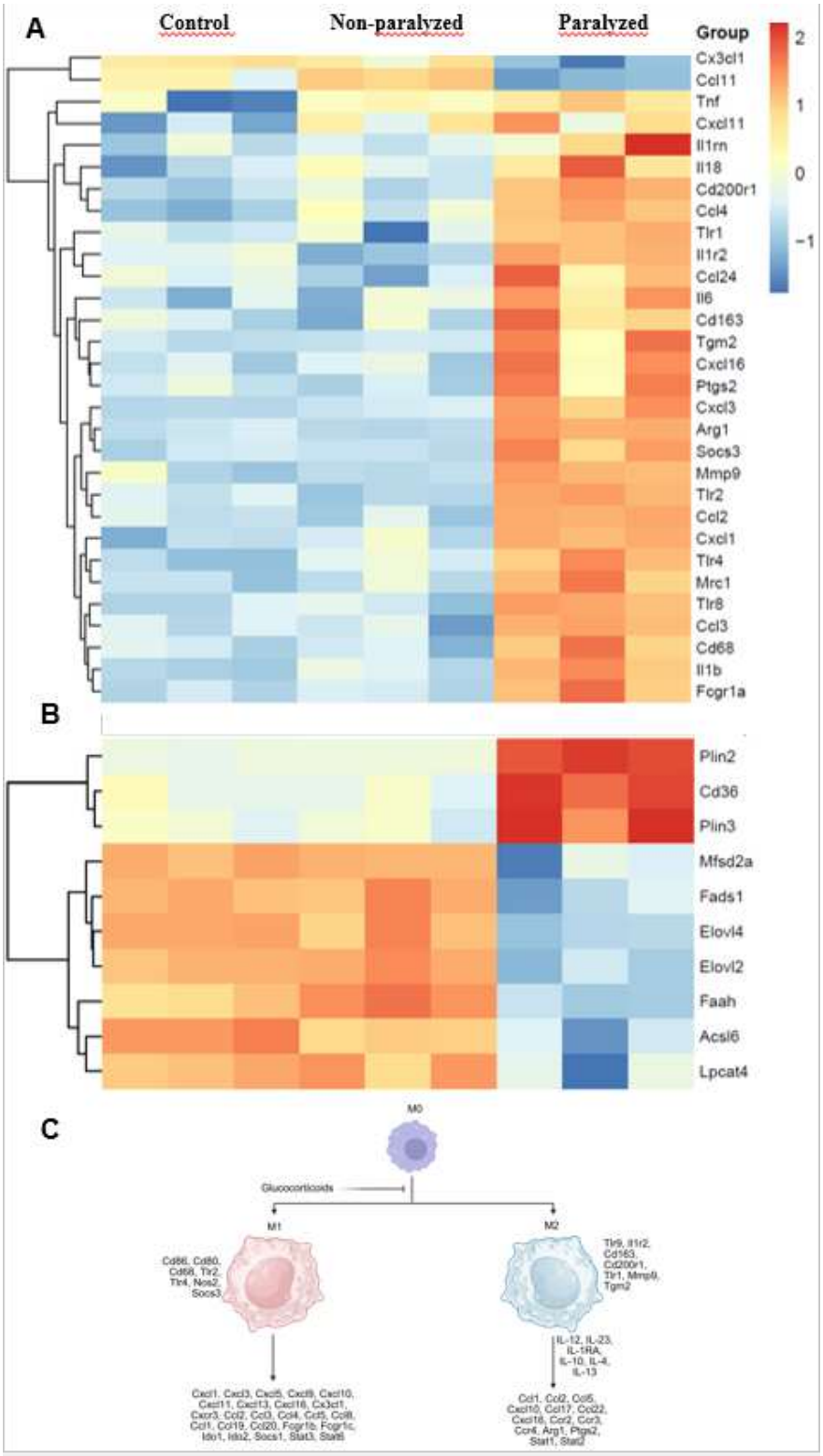


Figure 3

Fig. 3. Transcriptomic profiling of macrophage activation and DHA/EPA metabolic pathways at 24 h after ischemic spinal cord injury. (A,B) Gene-enrichment analysis identified increased expression of both M1- and M2-associated macrophage gene programs in paralyzed animals compared with uninjured controls and MES-stimulated non-paralyzed animals. The concurrent enrichment of both programs, without a clear separation into a predominant M1 or M2 phenotype, indicates an early and heterogeneous macrophage activation state following ischemic SCI. (B) Analysis of DHA/EPA-associated genes revealed increased expression of selected lipid-related and M2-associated markers, together with reduced expression of genes involved in the biosynthesis, uptake, transport, and intracellular retention of polyunsaturated fatty acids required for the generation of specialized pro-resolving mediators (SPMs). These findings suggest that, despite activation of macrophage-associated lipid programs, the injured SC exhibits a transcriptional constraint on the availability and metabolism of DHA/EPA substrates required for effective SPM biosynthesis. (C) Schematic representation of selected differentially expressed genesassociated with M1- and M2-associated macrophage programs and DHA/EPA metabolism, illustrating their relationships with inflammatory signaling, macrophage activation, lipid handling, and SPM biosynthetic pathways.

Supplementary Files

This is a list of supplementary files associated with this preprint. Click to download.

- MANUSCRIPTN110052026SIMATERIALrr.pdf
- MANUSCRIPTN110072026SIMATERIALLNrr.pdf
- MANUSCRIPTN110172026SIMATERIALLNrr.pdf